The EMBO Journal (2012) 31, 1379–1393 | © 2012 European Molecular Biology Organization | All Rights Reserved 0261-4189/12
www.embojournal.org

THE EMBO JOURNAL

Hypoxia regulates glutamate receptor trafficking through an HIF-independent mechanism

Since Advance Online Publication, this article has been corrected and a corrigendum is also printed in this issue.

Eun Chan Park[1,5], Piya Ghose[1,2,5], Zhiyong Shao[3], Qi Ye[3], Lijun Kang[4], XZ Shawn Xu[4], Jo Anne Powell-Coffman[3] and Christopher Rongo[1,*]

[1]Department of Genetics, The Waksman Institute, Rutgers The State University of New Jersey, Piscataway, NJ, USA, [2]The Graduate Program in Neuroscience, Rutgers The State University of New Jersey, Piscataway, NJ, USA, [3]Department of Genetics, Development and Cell Biology, Iowa State University, Ames, IA, USA and [4]The Life Sciences Institute, Department of Molecular & Integrative Physiology, University of Michigan, Ann Arbor, MI, USA

Oxygen influences behaviour in many organisms, with low levels (hypoxia) having devastating consequences for neuron survival. How neurons respond physiologically to counter the effects of hypoxia is not fully understood. Here, we show that hypoxia regulates the trafficking of the glutamate receptor GLR-1 in *C. elegans* neurons. Either hypoxia or mutations in *egl-9*, a prolyl hydroxylase cellular oxygen sensor, result in the internalization of GLR-1, the reduction of glutamate-activated currents, and the depression of GLR-1-mediated behaviours. Surprisingly, hypoxia-inducible factor (HIF)-1, the canonical substrate of EGL-9, is not required for this effect. Instead, EGL-9 interacts with the Mint orthologue LIN-10, a mediator of GLR-1 membrane recycling, to promote LIN-10 subcellular localization in an oxygen-dependent manner. The observed effects of hypoxia and *egl-9* mutations require the activity of the proline-directed CDK-5 kinase and the CDK-5 phosphorylation sites on LIN-10, suggesting that EGL-9 and CDK-5 compete in an oxygen-dependent manner to regulate LIN-10 activity and thus GLR-1 trafficking. Our findings demonstrate a novel mechanism by which neurons sense and respond to hypoxia.

The EMBO Journal (2012) **31,** 1379–1393. doi:10.1038/emboj.2011.499; Published online 17 January 2012
Subject Categories: membranes & transport; signal transduction; neuroscience
Keywords: *C. elegans*; glutamate; HIF; hypoxia; prolyl hydroxylase

Introduction

Aerobic organisms are sometimes confronted with an oxygen supply that is insufficient to meet the physiological demands of their cells, a state termed hypoxia. Hypoxia has a particularly strong impact on neurons, which are highly dependent on oxygen, have little in the way of glycolytic reserves, and are sensitive to excitotoxic death via overactivated glutamate receptors, including AMPA-type receptors (AMPARs) during ischaemic stroke (Buchan *et al*, 1991; Nellgard and Wieloch, 1992; Li and Buchan, 1993; Sheardown *et al*, 1993; Gill, 1994; Xue *et al*, 1994; Lees, 2000; Takahashi *et al*, 2002). In many species, neurons have mechanisms to combat oxygen deprivation and its consequences. For example, the cerebrocortical neurons of the freshwater painted turtle *Chrysemys picta bellii* can tolerate low oxygen, surviving months of oxygen deprivation during periods of winter dormancy by reducing GluR current amplitude, although the precise mechanism is unclear (Shin and Buck, 2003; Pamenter *et al*, 2008; Zivkovic and Buck, 2010). One possible hypoxia protection mechanism could involve regulated AMPAR trafficking, a process already known to mediate multiple forms of synaptic plasticity (Mammen *et al*, 1997; Lissin *et al*, 1998, 1999; 'O'Brien *et al*, 1998; Rongo and Kaplan, 1999; Shi *et al*, 1999; Hayashi *et al*, 2000), although such a protective role for trafficking has not been fully explored *in vivo*.

Metazoan cells in general use a well-studied and conserved hypoxia protection network. When oxygen levels are sufficiently high, the EGL-9/PHD family of prolyl hydroxylases use molecular oxygen, 2-oxoglutarate, and iron to hydroxylate key proline side chains on the hypoxia-inducible factor alpha (HIFα) proteins (Bruick and McKnight, 2001; Epstein *et al*, 2001; Fong and Takeda, 2008; Aragones *et al*, 2009). Once hydroxylated, HIFα is a substrate for the Von Hippel-Lindau (VHL) ubiquitin ligase, which ubiquitinates HIFα, targeting it for degradation. Under hypoxic conditions, HIFα protein remains stable, acting as a transcription factor to regulate gene expression (Fandrey and Gassmann, 2009; Semenza, 2009). Several studies have suggested that, as cellular oxygen sensors, EGL-9/PHD proteins might have other, less well-understood functions besides HIFα destabilization (Lee *et al*, 2005; Cummins *et al*, 2006; Fu *et al*, 2007; Koditz *et al*, 2007; Fu and Taubman, 2010).

Given that mammalian neurons in culture die so easily under hypoxia, it has been challenging to determine a cell biological link between hypoxia, the hypoxia response pathway, and AMPAR trafficking. Here, we have taken advantage of the genetically tractable and hypoxia tolerant model organism *C. elegans* to investigate how AMPAR trafficking is regulated in response to hypoxia. The *C. elegans* AMPAR subunits GLR-1 and GLR-2 act in the command interneurons to receive synaptic input and direct overall locomotory reversal behaviour (Hart *et al*, 1995; Maricq *et al*, 1995; Mellem *et al*, 2002; Chang and Rongo, 2005). Mutants that lack AMPAR function or fail to localize AMPARs at synapses have a depressed frequency of spontaneous reversals, and

*Corresponding author. Department of Genetics, Waksman Institute, Rutgers University, 190 Frelinghuysen Road, Piscataway, NJ 08854, USA. Tel.: +1 732 445 0955; Fax: +1 732 445 5735;
E-mail: rongo@waksman.rutgers.edu
[5]These authors contributed equally to this work

Received: 14 July 2011; accepted: 23 December 2011; published online: 17 January 2012; corrected: 10 February 2012

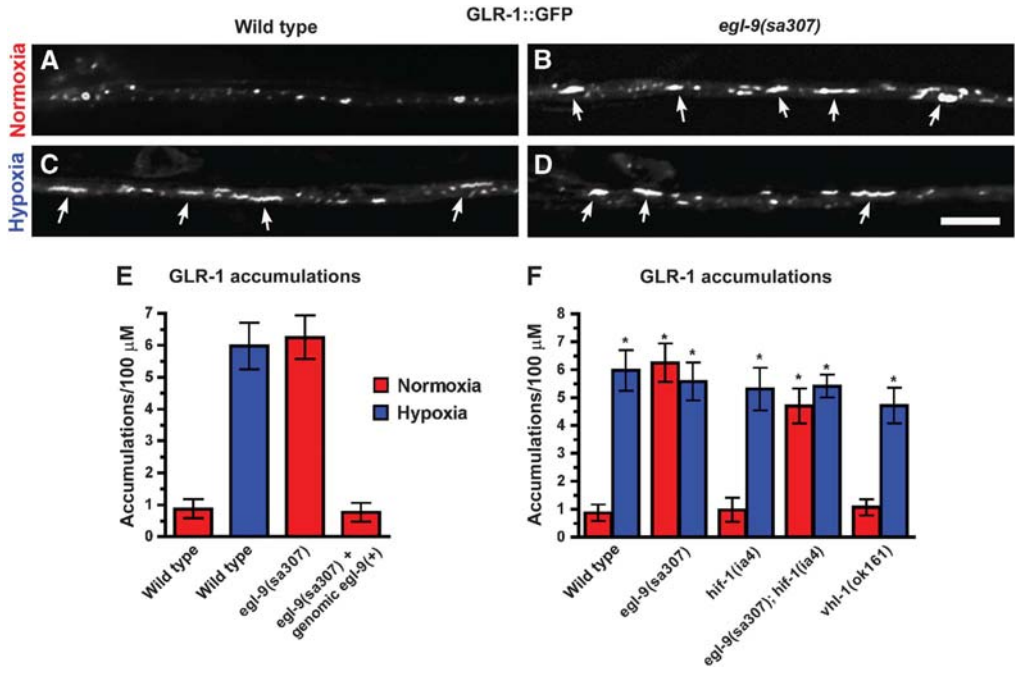

Figure 1 Oxygen levels and EGL-9 regulate GLR-1 trafficking. GLR-1::GFP fluorescence in (**A**) wild-type animals under normoxia, (**B**) *egl-9*(*sa307*) mutants under normoxia, (**C**) wild-type animals under hypoxia, and (**D**) *egl-9*(*sa307*) mutants under hypoxia. GLR-1 is localized to elongated accumulations (arrows), quantified per length of ventral cord dendrites in (**E**, **F**). Red bars indicate normoxia, whereas blue bars indicate hypoxia. ANOVA followed by Dunnett's multiple comparison with wild type, normoxia (*$P<0.01$). $N=15$–35 animals per condition and/or genotype. Error bars indicate s.e.m. Bar, 5 µm.

reversal frequency has been used to infer the abundance of AMPARs at synaptic membranes (Zheng *et al*, 1999; Burbea *et al*, 2002; Shim *et al*, 2004; Glodowski *et al*, 2005; Schaefer and Rongo, 2006). AMPAR synaptic trafficking has also been monitored directly *in vivo* using a GLR-1::GFP rescuing transgene (Rongo *et al*, 1998).

GLR-1 receptor synaptic abundance is regulated at the level of endocytosis and recycling (Burbea *et al*, 2002; Glodowski *et al*, 2007), and such regulation is used to modulate behaviour (Grunwald *et al*, 2004; Emtage *et al*, 2009). LIN-10, a PTB/PDZ domain protein homologous to mammalian Mints, mediates the recycling of endocytosed GLR-1 back to the plasma membrane, and *lin-10* mutants have GLR-1 receptors that remain trapped in endosomal compartments (Glodowski *et al*, 2007; Park *et al*, 2009). GLR-1 recycling is also regulated by the cyclin-dependent kinase CDK-5 and its p35 activator CDKA-1, which phosphorylate LIN-10, disrupting its subcellular localization and function (Juo *et al*, 2007).

Nematodes naturally encounter environmental conditions with variable oxygen concentrations, including hypoxia (Anderson and Dusenbery, 1977; Van Voorhies and Ward, 2000). Here, we show that hypoxia results in the retention of GLR-1 receptors in internal subcellular compartments. Loss of function mutations in *egl-9*, which encodes a PHD protein that normally inhibits the cellular response to hypoxia, mimics the effects of hypoxia on GLR-1 trafficking and depresses glutamate-activated currents and behavioural output. Unexpectedly, HIF-1, the canonical substrate of EGL-9 activity, is not required for this effect. Instead, EGL-9 interacts with LIN-10, a regulator of GLR-1 recycling. We show that oxygen levels control the subcellular localization of EGL-9 and LIN-10 in neurons, and the effect of hypoxia and *egl-9* mutations on LIN-10 localization and GLR-1 trafficking requires the activity of the CDK-5 kinase. Our results support a model in which EGL-9 and CDK-5 compete in an oxygen-dependent manner to regulate LIN-10 subcellular localization, GLR-1 membrane recycling, and GLR-1-mediated exploratory behaviour, demonstrating a novel mechanism by which neurons sense and respond to hypoxia.

Results

Hypoxia and EGL-9 regulate GLR-1 trafficking

In normoxia (room air: 21% oxygen), full-length, functional GLR-1 receptors tagged with GFP (GLR-1::GFP) are localized to discrete puncta along the ventral cord dendrites of interneurons (Figure 1A), with 85% of such puncta colocalized with synaptic markers (Rongo *et al*, 1998; Burbea *et al*, 2002). To determine if hypoxia alters GLR-1 trafficking, we incubated cultures of nematodes under hypoxic conditions using a published nitrogen displacement approach (Pocock and Hobert, 2008). We found that animals exposed to 0.5% oxygen (hypoxia) localized GLR-1::GFP to elongated accumulations along the ventral cord (Figure 1C), similarly to the GLR-1::GFP accumulation in enlarged endosomes observed in mutants for membrane recycling factors (Rongo *et al*, 1998; Glodowski *et al*, 2007; Park *et al*, 2009; Kramer *et al*, 2010; Shi *et al*, 2010). These GLR-1-containing compartments are distinct in shape and size (2.5 ± 0.5 µm) from >95% of the GLR-1 synaptic puncta (0.6 ± 0.2 µm) observed in normoxic wild-type animals, and thus can be easily distinguished and quantified (Figure 1E). The observed changes in GLR-1 localization are unlikely to be due to gross defects in synapse formation or overall cell polarity, as the localization of a synaptobrevin–GFP reporter (SNB-1::GFP), which decorates synaptic vesicles at interneuron presynaptic elements, does

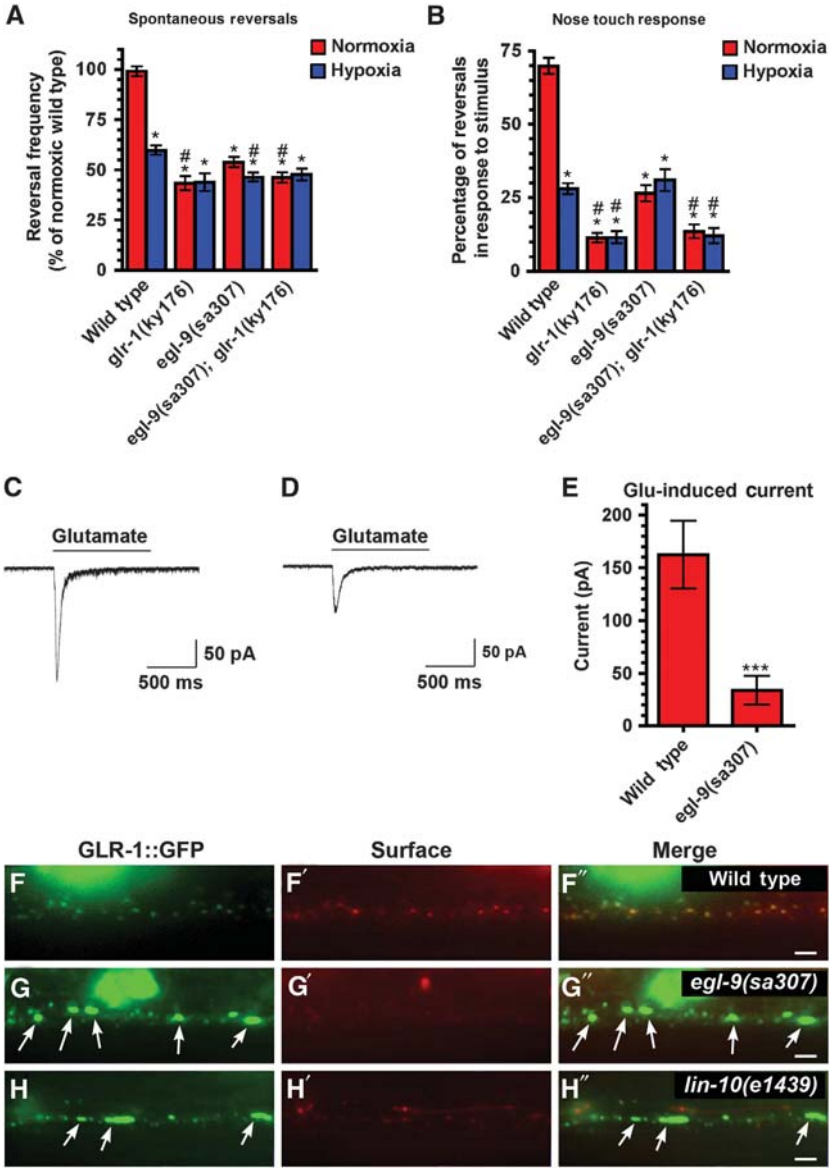

Figure 2 Oxygen levels and EGL-9 regulate GLR-1 function and locomotion behaviour. (**A**) The mean spontaneous reversal frequency (relative rate of spontaneous reversals in direction over a 5-min period) and (**B**) the mean nose touch mechanosensory response (percentage of reversal responses per animal to a train of 10 individual nose touch stimuli) are plotted for the indicated genotypes. Red bars indicate normoxia, whereas blue bars indicate hypoxia. ANOVA followed by Dunnett's multiple comparison with wild type, normoxia ($^{*}P<0.01$) or wild type, hypoxia ($^{\#}P<0.01$). $N=15$–35 animals per condition and/or genotype. (**C**, **D**) Representative whole-cell recordings from AVA neurons are plotted. Example inward currents induced by glutamate application (bar) over time are plotted for (**C**) a wild-type neuron and (**D**) an *egl-9*(*sa307*) mutant neuron. (**E**) Mean peak current amplitudes for wild-type and *egl-9*(*sa307*) mutants. Student's *t*-test ($^{***}P<0.001$). $N=6$–9 animals per genotype. (**F**–**H**) Fluorescence from the ventral nerve cords of HA::GLR-1::GFP transgenic animals following injection of anti-HA antibodies (conjugated to Alexa 594) into the extracellular body cavity under non-membrane permeabilizing conditions. Injections were performed on (**F**) wild-type, (**G**) *egl-9*(*sa307*) mutants, and (**H**) *lin-10*(*e1439*) mutants. (**F**–**H**) Total GFP fluorescence. (**F′**, **G′**, **H′**) Alexa 594 fluorescence detecting surface HA::GLR-1::GFP decorated with anti-HA antibodies. (**F″**, **G″**, **H″**) Merged images. Arrows point to elongated, internal compartments that accumulate HA::GLR-1::GFP and that cannot be decorated by anti-HA antibodies in *egl-9* and *lin-10* mutants. Error bars indicate s.e.m. Bar, 5 μm.

not change upon shift from normoxia to hypoxia (Supplementary Figure S1A–C). In addition, we detected similar levels of *glr-1* mRNA in hypoxic and normoxic animals, indicating that the observed changes are post-transcriptional (Supplementary Figure S1D).

We reasoned that hypoxia might be activating the PHD/HIF pathway to regulate GLR-1. If this were the case, then mutations in the lone *C. elegans* PHD gene *egl-9* should cause a similar effect in normoxic animals to that seen in hypoxic wild-type animals. We examined GLR-1::GFP in two strong loss of function *egl-9* mutants: *egl-9*(*sa307*) and *egl-9*(*n571*) (Darby *et al*, 1999). Both mutations caused GLR-1 to be localized to elongated accumulations similar to those seen in hypoxic animals (Figure 1B and E; Supplementary Figure S1E and F). As in hypoxic animals, *egl-9* mutants had an SNB-1::GFP punctate pattern similar to that of wild-type animals (Supplementary Figure S1A–C), and similar levels of *glr-1* mRNA (Supplementary Figure S1D). Introduction of a wild-type *egl-9* transgene fully rescued the GLR-1 localization defects of *egl-9* mutants (Figure 1E). Interestingly, there was

no additive effect of combining *egl-9* mutations with hypoxia (Figure 1D and F), suggesting that the effect of hypoxia on GLR-1 is through EGL-9.

EGL-9 regulates multiple developmental and behavioural processes, each of which depends on HIF-1 function (Shen *et al*, 2006; Chang and Bargmann, 2008; Gort *et al*, 2008; Pocock and Hobert, 2008; Shao *et al*, 2010). If HIF-1 were also involved in regulating GLR-1 trafficking, then the effects of hypoxia or *egl-9* mutations on GLR-1 trafficking should be suppressed by a deletion mutation in *hif-1*. We examined GLR-1::GFP in a *hif-1* molecular null (Jiang *et al*, 2001). Surprisingly, this *hif-1* mutation did not alter the GLR-1 trafficking defects of hypoxic animals or *egl-9* mutants, and did not affect GLR-1 under normoxic conditions (Figure 1F). We also examined the GLR-1 localization phenotype in mutants that are deficient for VHL-1 and RHY-1, as they inhibit HIF-1 (Epstein *et al*, 2001; Shen *et al*, 2006). Loss of function mutations in these genes did not affect GLR-1 localization (Figure 1F; Supplementary Figure S1E and F). Collectively, these data strongly suggest that EGL-9 and hypoxia regulate GLR-1 subcellular localization by a novel pathway.

Hypoxia and EGL-9 regulate GLR-1 function

The elongated accumulations of GLR-1 in hypoxic animals and *egl-9* mutants are similar to those observed in mutants in which GLR-1 recycling is impaired, suggesting that they might represent internalized receptors. If this were the case, then synapses should be partially depleted of GLR-1 and thus depressed for GLR-1 function. We tested this several different ways. First, we monitored functional synaptic GLR-1 by measuring two GLR-1-mediated behaviours: the frequency of spontaneous reversals in locomotion during foraging and the frequency of reversals in response to nose touch stimuli (i.e., nose touch mechanosensation). Both hypoxic animals and normoxic *egl-9* mutants showed depressed reversal rates and depressed nose touch mechanosensation rates compared with those of wild-type animals in normoxia, although not quite as severe as those observed in *glr-1* null mutants (Figure 2A and B). Thus, hypoxic conditions repress GLR-1-dependent behaviours. Double mutants between *egl-9* and *glr-1* resembled *glr-1* single mutants, consistent with EGL-9 regulating these behaviours in the same genetic pathway as GLR-1 (Figure 2A and B). Mutations in *hif-1* did not affect reversal behaviour, nor did they suppress the effect of *egl-9* mutations or hypoxia on reversal behaviour (Supplementary Figure S1G), indicating that this role of EGL-9 is independent of HIF-1.

Second, we directly tested whether EGL-9 can influence GLR-1 channel activity. Glutamate-activated currents can be recorded from the interneuron AVA (Mellem *et al*, 2002). If endogenous GLR-1 is retained internally (internalized) in *egl-9* mutants, then mutant interneurons should have reduced glutamate-activated currents. We used a previously described whole-cell recording protocol to measure the size of GLR-1-mediated currents in the AVA interneuron elicited by the application of 1 mM glutamate (Wang *et al*, 2010), and we found that there was a significant reduction in current amplitude in *egl-9* versus wild type when AVA was voltage clamped at −70 mV (Figure 2C–E). Current–voltage relationship in neurons from wild-type animals and *egl-9* mutants did not differ, indicating that *egl-9* mutants do not have general defects in conductance (Supplementary Figure S1H).

Third, we directly examined the amount of GLR-1 receptors exposed on the plasma membrane by performing cell surface antibody labelling (Gottschalk and Schafer, 2006). We examined transgenic animals that express GLR-1 dual-tagged with an extracellular HA epitope and an intracellular GFP (Wang *et al*, 2008). Using anti-HA antibodies under non-permeabilized conditions, we detected both total HA::GLR-1::GFP (Figure 2F) and membrane surface receptor (Figure 2F′) in wild type. By contrast, we detected little surface HA::GLR-1::GFP in *egl-9* mutants (Figure 2G′), even though significant levels of HA::GLR-1::GFP were present (Figure 2G). Taken together, our results indicate that GLR-1 receptors accumulate in elongated, internal compartments along dendrites of *egl-9* mutants.

A specific EGL-9 isoform regulates GLR-1 trafficking

EGL-9 might have multiple molecular or biochemical functions, as the *egl-9* gene produces a number of different protein isoforms (Figure 3A). We tested whether a specific EGL-9 isoform regulates GLR-1 trafficking by generating multiple isoform-specific transgenes, each under the control of the *glr-1* promoter, and testing them for their ability to rescue the GLR-1 localization phenotype of *egl-9* mutants. We found that isoform EGL-9E, which lacks the first two exons, completely rescued both the GLR-1 localization phenotype and the behavioural defects of *egl-9* mutants (Figure 3B–G). By contrast, both isoforms EGL-9A, which is the longest isoform, and EGL-9C, which lacks exons 1–4, failed to rescue the GLR-1 trafficking defects of *egl-9* mutants (Figure 3C).

Figure 3 A specific EGL-9 isoform regulates GLR-1 trafficking. (**A**) Schematic of *egl-9* genomic DNA organization, the three predominant splice isoforms that are produced, and the coding sequences for the 'catalytic domain' transgene that we generated. Boxes indicate coding sequences within exons. The arrows indicate the start sites of transcription for the three different isoforms. Brackets indicate regions that encode the indicated protein domains, the boxes for which have also been colour coded. The red lines indicate the regions of genomic DNA deleted in *gk277* and *sa307* mutants. The locations of amino-acid substitutions are indicated for *n571* and the H487 residue mutated in the catalytically impaired EGL-9 transgene. GLR-1::GFP fluorescence in (**B**) wild-type, (**E**) *egl-9* mutants, and *egl-9* mutants expressing the (**F**) EGL-9A, (**G**) EGL-9E, and (**H**) EGL-9E(H487A) isoforms via the *glr-1* promoter. Arrows point to accumulations of GLR-1::GFP in elongated compartments. (**C**) Quantification of the number of elongated, internal compartments of accumulated GLR-1::GFP detected in the indicated genotypes. (**D**) The mean spontaneous reversal frequency as an indication of GLR-1 function is plotted for the indicated genotypes. For (**C**) and (**D**), ANOVA followed by Dunnett's multiple comparison with wild type (*$P<0.01$). (**I–N**) Cell body (left panel) and ventral cord (right panel) fluorescence from animals expressing (**I**) an EGL-9A::GFP chimera, (**L**) an EGL-9E::GFP chimera, (**M**) an EGL-9C::GFP chimera, and (**N**) a chimera containing GFP fused to just the catalytic domain of EGL-9. (**J**) Quantification of the number of fluorescent puncta along the ventral cord generated from the indicated transgene. ANOVA followed by Dunnett's multiple comparison with (**J**) GFP::EGL-9A (*$P<0.01$). (**K**) Quantification of the number of GFP::EGL-9E fluorescent puncta along the ventral cord under conditions of normoxia (red) and hypoxia (blue). Student's *t*-test, (***$P<0.001$). $N=15$–30 animals per condition and/or genotype. Error bars indicate s.e.m. Bar, 5 μm.

We also tested the localization pattern of the different EGL-9 isoforms by tagging them with GFP and examining their subcellular localization in interneurons. EGL-9A and EGL-9C, which failed to rescue GLR-1 trafficking defects, were localized to nuclei, but were diffusely distributed throughout ventral cord dendrites (Figure 3I–M). By contrast, EGL-9E, which rescues GLR-1 trafficking defects, was localized to puncta along the ventral cord (Figure 3J and L) in addition

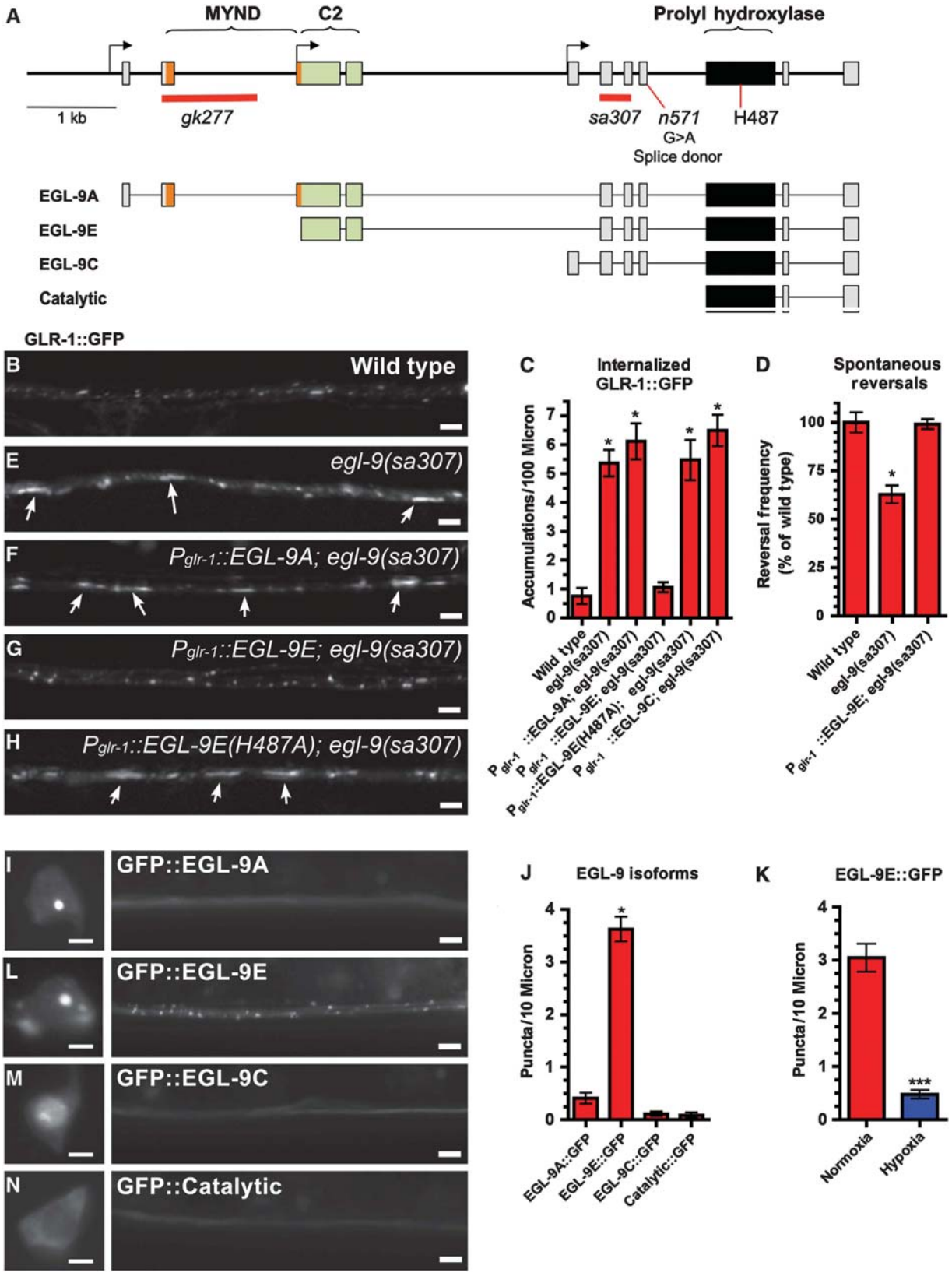

to the nucleus. We noted that EGL-9E contains exons 3 and 4, which are not found in EGL-9C, suggesting that the sequences encoded by these exons might be critical for localizing EGL-9E to puncta in neurons. We analysed the sequence of exons 3 and 4, and found that it encodes a potential C2 domain (Supplementary Figure S2), which could be mediating protein–protein or protein–phospholipid interactions (Rizo and Sudhof, 1998). Taken together, our results suggest that, in addition to the prolyl hydroxylase catalytic domain, EGL-9 contains additional protein domains that can conduct specialized functions, including the direction of subcellular localization. We also speculate that the amino acids encoded by exons 1 and 2 antagonize EGL-9 punctate localization in neurons (mediated by the C2 domain in exons 3 and 4).

To examine the role of oxygen sensation in the regulation of GLR-1 trafficking, we tested the importance of EGL-9E catalytic function. The prolyl hydroxylase catalytic domain is an oxygen sensor comprising histidine and arginine side chains that stably bind to 2-oxoglutarate and iron, which in turn interact with molecular oxygen (Epstein *et al*, 2001; McDonough *et al*, 2006; Chowdhury *et al*, 2009). We therefore treated animals with the iron chelator 2,2′-dipyridyl (DIP) and found that such treatment resulted in the accumulation of GLR-1::GFP in internal compartments similarly to those observed in *egl-9* mutants and hypoxic animals (Supplementary Figure S1E and F). Next, we tested the ability of EGL-9E(H487A) to rescue the GLR-1 localization phenotype of *egl-9* mutants. Histidine 487 (amino-acid numbering based on the longest EGL-9 isoform) is a highly conserved residue that coordinates iron in the catalytic core and is required for EGL-9 to regulate HIF-1; the equivalent mutation in mammalian PHD2 reduces iron binding, hydroxylase activity, and oxygen sensing (McDonough *et al*, 2006; Shao *et al*, 2009). We found that EGL-9E(H487A) failed to rescue (Figure 3C and H). Finally, we examined the role of oxygen on EGL-9E subcellular localization. We found that hypoxia resulted in a decrease in the number of EGL-9E puncta in the ventral cord (Figure 3K). Our findings indicate that EGL-9E catalytic activity is required to regulate GLR-1 trafficking, and that oxygen can regulate the subcellular localization of EGL-9E itself.

EGL-9 interacts with LIN-10

To identify the substrates of EGL-9 that regulate GLR-1, we generated a yeast two-hybrid bait plasmid containing just the catalytic domain of EGL-9 (amino acids 347–608) and used it to screen a *C. elegans* prey cDNA library, identifying LIN-10, a PDZ/PTB domain protein of the Mint family and a known mediator of GLR-1 membrane recycling (Rongo *et al*, 1998; Glodowski *et al*, 2007; Park *et al*, 2009). To characterize the interaction between LIN-10 and EGL-9, we generated a collection of yeast two-hybrid prey vectors containing different regions of the LIN-10 protein, and then examined the ability of these preys to support the expression of multiple markers when paired with the EGL-9 catalytic domain as bait. We found that amino acids 1–138 of LIN-10 showed a strong interaction with EGL-9, and that amino acids 1–90 as well as amino acids 108–280 were capable of weak interactions with EGL-9, suggesting that the amino-terminus of LIN-10 might contain multiple sites for EGL-9 interaction (Figure 4A).

To explore whether EGL-9 regulates GLR-1 through its interaction with LIN-10, we re-examined GLR-1 localization in *lin-10* mutants. Like in hypoxic animals (Figure 4D) and *egl-9* mutants, GLR-1::GFP accumulates in elongated, internal compartments in *lin-10* mutants (Figure 4C), although at higher numbers (Figure 4F). Similarly, mutants for *lin-10* demonstrate behavioural defects consistent with diminished GLR-1 function (Figure 4M and N). We used cell surface antibody labelling to directly examine the amount of HA::GLR-1::GFP on the plasma membrane of *lin-10* mutants, but detected little surface HA::GLR-1::GFP (Figure 2H′). We also examined *lin-10* single mutants and *egl-9 lin-10* double mutants under conditions of either normoxia or hypoxia. Neither hypoxia treatment nor *egl-9* mutations increased the severity of the GLR-1 localization and behavioural defects in animals lacking LIN-10, suggesting that LIN-10 and EGL-9 act in the same genetic pathway to regulate oxygen-sensitive GLR-1 trafficking (Figure 4F, M, and N; Supplementary Figure S1E and F). Finally, if EGL-9 interacts with LIN-10, then we might expect both proteins to be colocalized in neurons. We examined GFP::EGL-9E and LIN-10::mCherry in interneuron cell bodies (Figure 4G, I, and K) and dendrites (Figure 4H, J, and L), and found that the two proteins were colocalized to puncta.

EGL-9 could require its interaction with LIN-10 solely to regulate GLR-1, or alternatively LIN-10 could be essential for all EGL-9-dependent functions, including its regulation of HIF-1 protein levels and the hypoxia response. We tested these possibilities by examining several phenotypes of *egl-9*(*sa307*) that are rescued by EGL-9A (Epstein *et al*, 2001; Shao *et al*, 2009). First, we measured HIF-1 protein levels and found that they were not altered in *lin-10* mutants (Supplementary Figure S3A). Second, we found that *lin-10* mutations did not affect HIF-1 levels in mutants for the VHL-1 ubiquitin ligase, which targets HIF-1 for degradation (Supplementary Figure S3A). Third, we found that expression from $P_{nhr\text{-}57}$::*GFP*, a reporter for HIF-1-dependent transcription

Figure 4 EGL-9 interacts with LIN-10 to regulate GLR-1 trafficking. (**A**) Schematic of LIN-10 protein. Coloured boxes indicate the CID, PTB, PDZ1, and PDZ2 domains. Vertical lines indicate putative CDK-5 phosphorylation sites in the amino-terminus, with the number corresponding to the proline residue in the CDK-5 consensus sequence. Horizontal lines indicate the fragments of LIN-10 protein tested for interaction with the EGL-9 catalytic domain via yeast two-hybrid. '+++' Indicates a strong interaction (positive for all four reporters), whereas '+' indicates a weak interaction (positive for 1–3 reporters). GLR-1::GFP fluorescence in (**B**) wild type, normoxia; (**C**) *lin-10*(*e1439*), normoxia; (**D**) wild type, hypoxia; and (**E**) *lin-10*(*e1439*), hypoxia. Arrows indicate accumulations of GLR-1::GFP in elongated, internal compartments. (**F**) Quantification of the number of GLR-1::GFP-containing elongated compartments in the indicated genotypes. $^{*}P<0.01$ compared with wild type, normoxia, and $^{\#}P<0.01$ compared with wild type, hypoxia, by ANOVA followed by Dunnett's multiple comparison. (**G**, **H**) GFP::EGL-9E fluorescence and (**I**, **J**) LIN-10::mCherry fluorescence in (**G**, **I**, **K**) a neuron cell body (PVC) and (**H**, **J**, **L**) the ventral cord. (**K**, **L**) Merged images. (**M**) The mean spontaneous reversal frequency and (**N**) the mean nose touch mechanosensory response are plotted for the indicated genotypes. Red bars indicate normoxia, whereas blue bars indicate hypoxia. ANOVA followed by Dunnett's multiple comparison with wild type, normoxia ($^{*}P<0.01$) or wild type, hypoxia ($^{\#}P<0.01$). $N=20$–30 animals per condition and/or genotype. Error bars indicate s.e.m. Bar, 5 μm.

during hypoxia that shows elevated expression in both *egl-9* and *vhl-1* mutants (Shen *et al*, 2006), did not significantly change in *lin-10* mutants relative to wild type under both normoxic and hypoxic conditions (Supplementary Figure S3B–D). Our results indicate that LIN-10 is not required for the canonical HIF-1 hypoxia response pathway.

EGL-9 and CDK-5 regulate LIN-10 subcellular localization

The LIN-10 amino-terminus directs LIN-10 subcellular localization to Golgi and endosomal puncta (Whitfield *et al*, 1999; Glodowski *et al*, 2005; Park *et al*, 2009). Since EGL-9 binds to the LIN-10 amino-terminus, we reasoned that EGL-9 and oxygen might regulate LIN-10 subcellular localization along

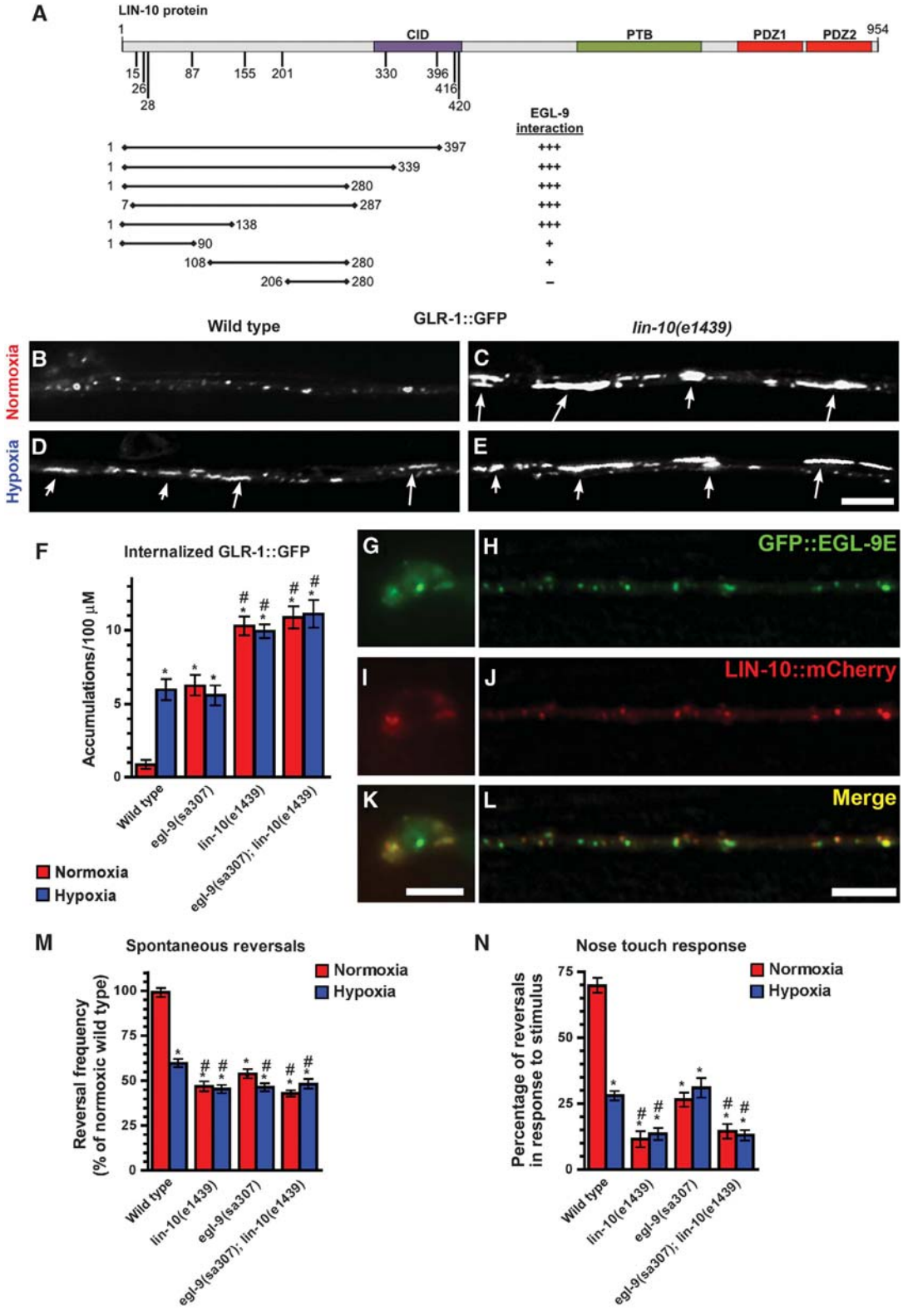

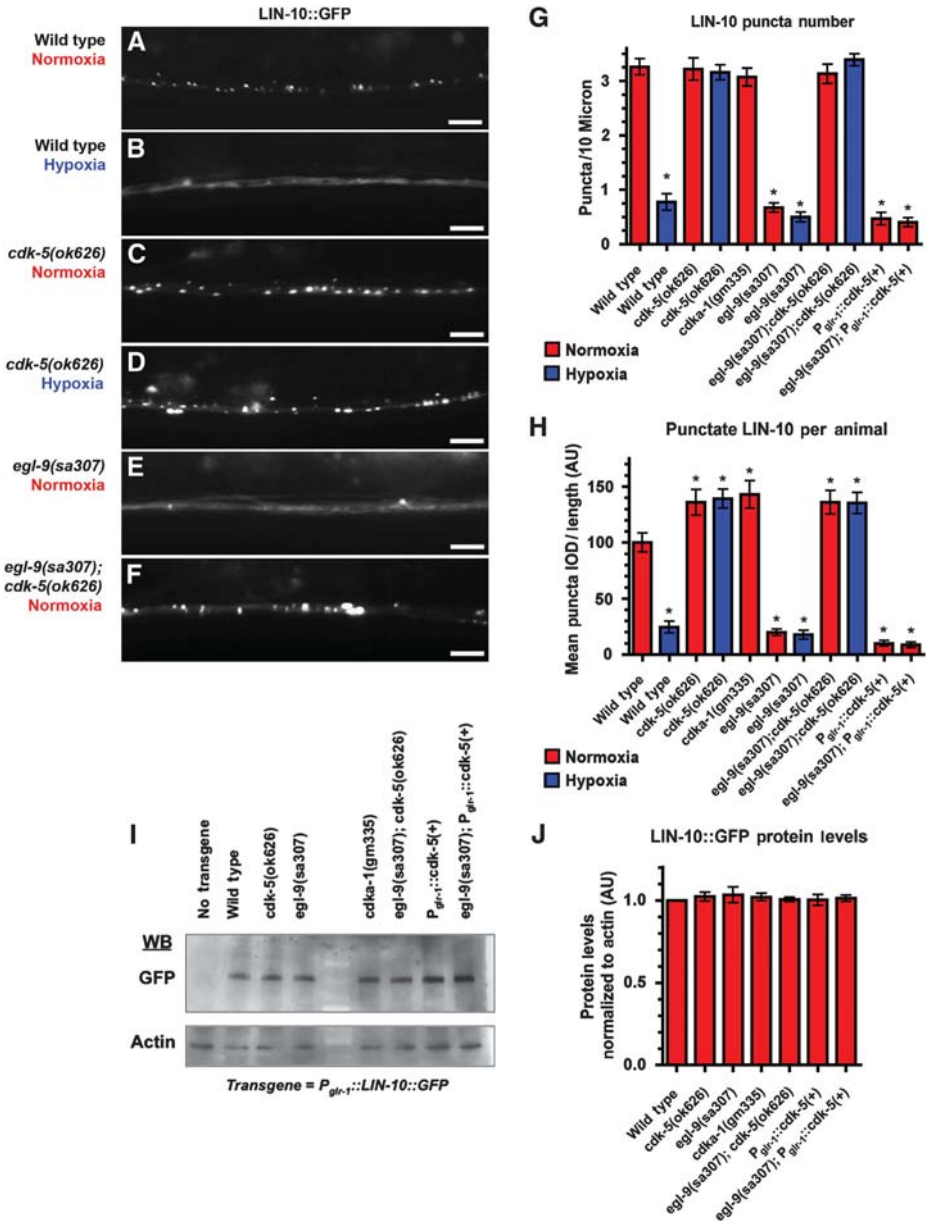

Figure 5 EGL-9 and CDK-5 regulate LIN-10 subcellular localization. LIN-10::GFP ventral cord fluorescence for (**A**) wild type, normoxia; (**B**) wild type, hypoxia; (**C**) *cdk-5*(*ok626*), normoxia; (**D**) *cdk-5*(*ok626*), hypoxia; (**E**) *egl-9*(*sa307*), normoxia; and (**F**) *egl-9 cdk-5* double mutants, normoxia. Quantification of LIN-10::GFP (**G**) puncta number per length of ventral cord and (**H**) integrated optical density (IOD) per puncta per animal. IOD is the sum of the pixel values for each puncta, reflecting both puncta size and fluorescence intensity. Red bars indicate normoxia, whereas blue bars indicate hypoxia. ANOVA followed by Dunnett's multiple comparison with wild type, normoxia (*$P<0.01$). (**I**) Representative western blot detecting LIN-10::GFP using anti-GFP antibodies (top panel) or actin using anti-actin antibodies (bottom panel) from nematode lysates of the given genotype. With the exception of the first lane, all nematodes carried the *odIs22[*$P_{glr\text{-}1}$*::LIN-10::GFP]* transgene. (**J**) Quantification of LIN-10::GFP protein levels normalized to actin controls from the same blot. Means represent five independent blots. $N=15$–35 animals per condition and/or genotype. Error bars indicate s.e.m. Bar, 5 μm.

dendrites. We found that LIN-10::GFP resides at puncta under normoxic conditions (Figure 5A), whereas it is diffusely distributed throughout dendrites under hypoxic conditions (Figure 5B). We quantified this effect by measuring the number of LIN-10::GFP puncta (Figure 5G) and the size and fluorescence intensity of LIN-10::GFP puncta as a combined integrated optical density (IOD), summing the pixel values for each punctum, which were then totalled for each animal (Figure 5H). We also examined LIN-10::GFP in *egl-9* mutants and found a diffuse distribution of LIN-10 similar to that of hypoxic animals (Figure 5E, G, and H). Our quantification of LIN-10::GFP fluorescence suggests that LIN-10 shifts from endosomal localization to a cytosolic distribution in *egl-9* mutants. To confirm that this change in LIN-10 localization indicates a redistribution of LIN-10 rather than a loss of LIN-10 protein levels in *egl-9* mutants, we examined LIN-10::GFP protein levels in nematodes by western blot, using transgenic animals that only express LIN-10::GFP in the GLR-1-expressing interneurons (Figure 5I). Relative to actin levels, we did not detect a significant change in LIN-10 protein levels in *egl-9* mutants compared with wild type (Figure 5J), indicating that EGL-9 does not regulate LIN-10 protein levels.

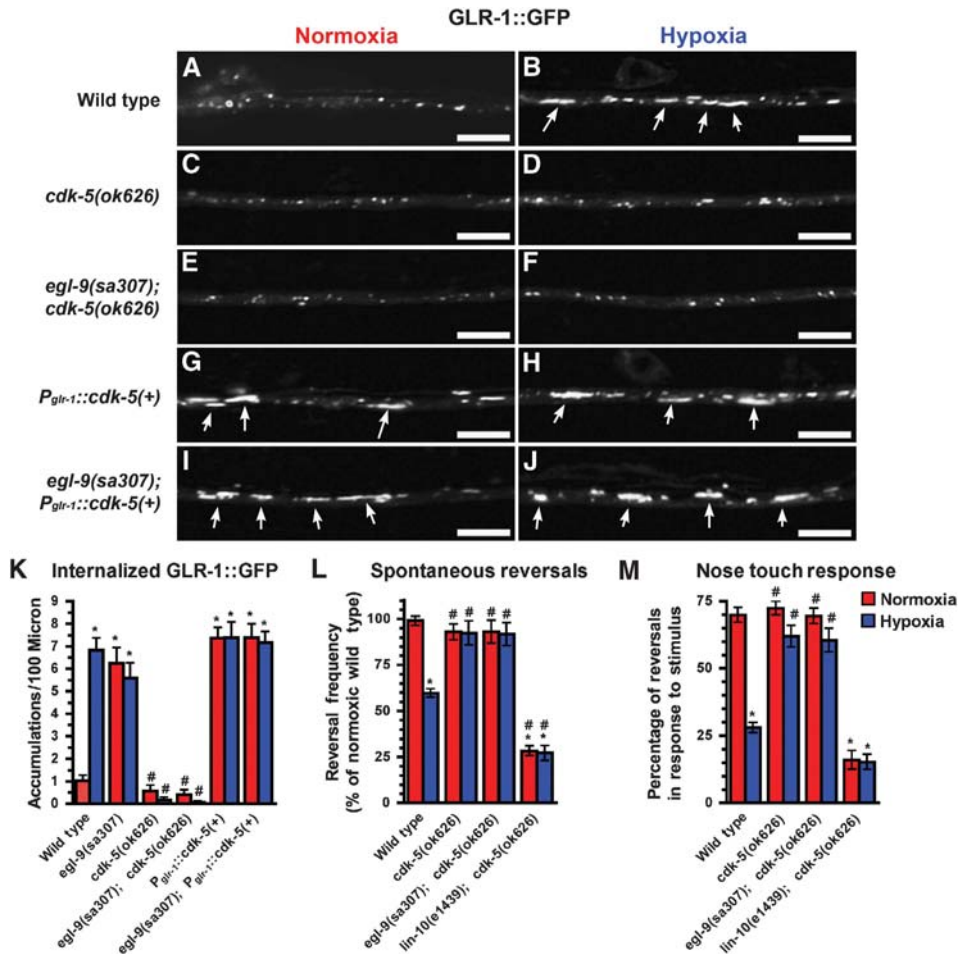

Figure 6 CDK-5 is required for oxygen and EGL-9 to regulate GLR-1 trafficking. GLR-1::GFP ventral cord fluorescence for (**A**, **B**) wild-type, (**C**, **D**) *cdk-5*(*ok626*), (**E**, **F**) *egl-9 cdk-5* double mutants, (**G**, **H**) wild type overexpressing wild-type CDK-5, and (**I**, **J**) *egl-9*(*sa307*) overexpressing wild-type CDK-5 under conditions of (**A**, **C**, **E**, **G**, **I**) normoxia or (**B**, **D**, **F**, **H**, **J**) hypoxia. Arrows indicate accumulations of GLR-1::GFP in internalized compartments. (**K**) Quantification of the number of GLR-1::GFP-containing elongated compartments in the indicated genotypes. (**L**) The mean spontaneous reversal frequency and (**M**) the mean nose touch mechanosensory response are plotted for the indicated genotypes. Red bars indicate normoxia, whereas blue bars indicate hypoxia. $^{*}P<0.01$ compared with wild type, normoxia, and $^{\#}P<0.01$ compared with wild type, hypoxia, by ANOVA followed by Dunnett's multiple comparison. $N=15$–35 animals per condition and/or genotype. Error bars indicate s.e.m. Bar, 5 μm.

The amino-terminus of LIN-10 also interacts with the proline-directed serine-threonine kinase CDK-5, which negatively regulates LIN-10 by phosphorylating multiple proline-proximal sites on the amino-terminus (Juo *et al*, 2007). As EGL-9 can hydroxylate prolines, we reasoned that EGL-9 could prevent the inhibitory phosphorylation of LIN-10 by CDK-5, thereby keeping LIN-10 active. If correct, then loss of CDK-5 should protect LIN-10 from hypoxia-mediated down-regulation. We tested this model by first examining LIN-10::GFP localization in *cdk-5* mutants. We found that LIN-10::GFP was localized to puncta in *cdk-5* and *cdka-1* mutants under both normoxic and hypoxic conditions (Figure 5C, D, G, and H). We also examined LIN-10::GFP in *egl-9 cdk-5* double mutants and found that LIN-10 was localized to puncta in a manner similar to that of *cdk-5* single mutants (Figure 5F–H). LIN-10::GFP protein levels remained constant in these genotypes (Figure 5I and J). Our results indicate that the regulation of LIN-10::GFP subcellular localization by hypoxia and EGL-9 requires the activity of CDK-5.

If EGL-9 promotes LIN-10 function by antagonizing the ability of CDK-5 to phosphorylate LIN-10, then we would expect that the loss of CDK-5 would block the effects of hypoxia and *egl-9* mutations on GLR-1 trafficking. Whereas hypoxia caused wild-type neurons to accumulate GLR-1 in internal compartments (Figure 6A and B), mutations in *cdk-5* completely blocked this effect (Figure 6C, D, and K). In addition, mutations in *cdk-5* suppressed the GLR-1 trafficking defects caused by *egl-9* mutations (Figure 6E, F, and K). Consistent with the GLR-1 trafficking data, we observed that mutation in *cdk-5* suppressed the spontaneous reversal and nose touch mechanosensation behavioural defects in both hypoxic wild-type animals and *egl-9* mutants (Figure 6L and M), placing CDK-5 genetically downstream of EGL-9 and oxygen. Importantly, mutations in *cdk-5* did not suppress the defects in GLR-1 trafficking and GLR-1-mediated behaviours observed in *lin-10* mutants (Figure 6L and M; data not shown), indicating that LIN-10 is acting genetically downstream of CDK-5.

We introduced a transgene, $P_{glr\text{-}1}$::*cdk-5*(+), into nematodes to overexpress wild-type CDK-5 (Juo *et al*, 2007). Overexpression of wild-type CDK-5 results in a phenotype similar to that of *egl-9* mutants and hypoxic animals (Figure

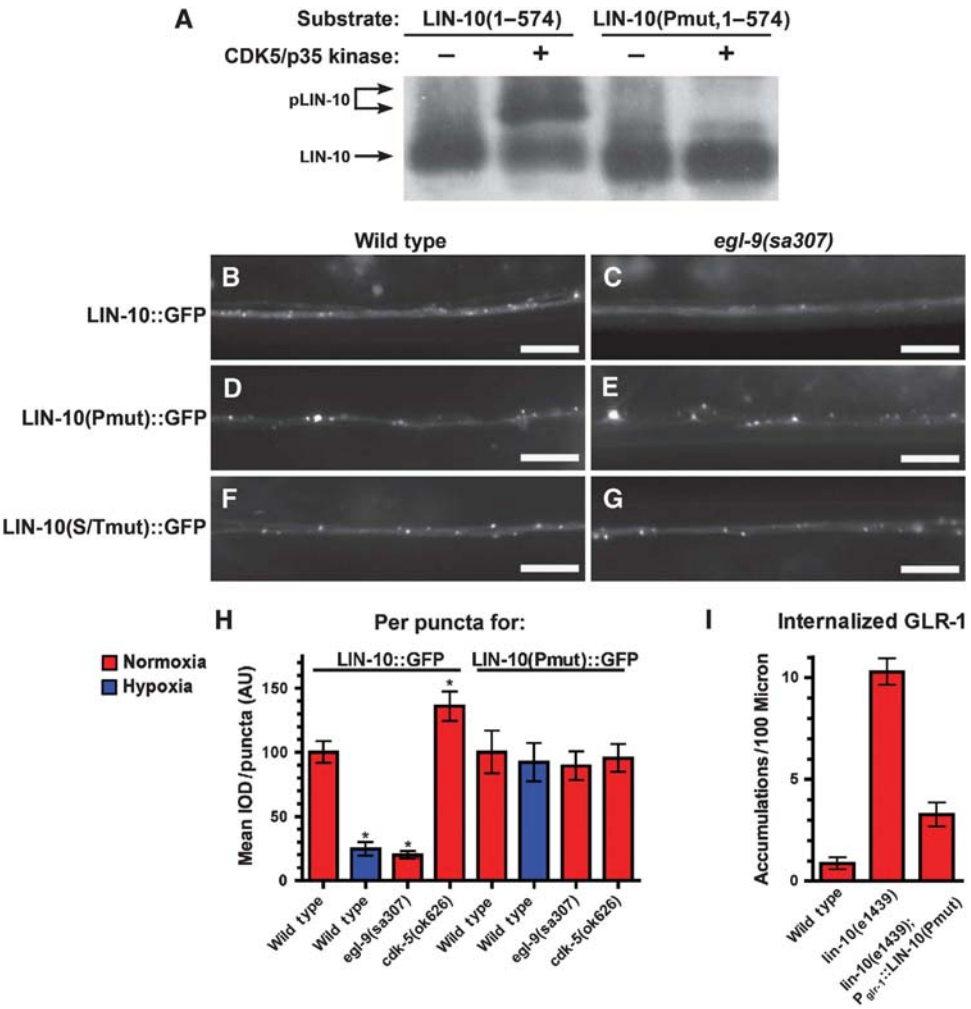

Figure 7 Proline-rich CDK-5 consensus sequences regulate LIN-10 localization. (**A**) Phos-tag western blot detecting *in-vitro* translated phosphorylated LIN-10 protein (upper bands) or unphosphorylated LIN-10 protein (lower band). Specific substrates (the first 574 amino acids of wild-type LIN-10 or LIN-10(Pmut), which contains proline to alanine substitutions in the CDK-5 consensus sequences) after incubation with CDK-5 kinase (indicated by '+') or buffer alone (indicated by '−'). Ventral cord fluorescence for (**B**, **C**) wild-type LIN-10::GFP, (**D**, **E**) LIN-10(Pmut)::GFP, with the proline mutations indicated above, or (**F**, **G**) LIN-10(S/Tmut)::GFP, with the serine or threonine substituted to alanine in the CDK-5 consensus sequences. (**H**) Quantification of LIN-10::GFP or LIN-10::GFP(Pmut)::GFP integrated optical density (IOD) per puncta for the indicated genotypes. IOD is the sum of the pixel values for each puncta, reflecting both puncta size and fluorescence intensity. Red bars indicate normoxia, whereas blue bars indicate hypoxia. ANOVA followed by Dunnett's multiple comparison with wild type, normoxia ($^*P<0.01$). (**I**) Quantification of GLR-1::GFP-containing compartments in the indicated genotypes, including *lin-10* mutants expressing an untagged version of LIN-10(Pmut). $N=15$–30 animals per condition and/or genotype. Error bars indicate s.e.m. Bar, 5 μm.

6G, H, and K). Interestingly, CDK-5 was not able to increase the amount of internalized GLR-1 when overexpressed in *egl-9* mutants, hypoxic animals, or a combination of both (Figure 6I–K), indicating that the effect of CDK-5 overexpression is not additive with the effects of *egl-9* mutations or hypoxia, consistent with CDK-5 and EGL-9 regulating the same target. Our results show that in the absence of EGL-9 function or oxygen, CDK-5 overly depresses GLR-1 recycling, suggesting that EGL-9 and CDK-5 normally compete against each other to regulate GLR-1 trafficking.

EGL-9 could regulate LIN-10 localization by preventing LIN-10 phosphorylation by CDK-5, perhaps by hydroxylating prolines within each CDK-5 phosphorylation consensus site. In this model, we would predict that removing the proline residues from these consensus sites would block the phosphorylation of LIN-10 by CDK-5. Ten putative CDK-5 phosphorylation sites (serine or threonine with an adjacent proline) are located in the LIN-10 amino-terminus (Figure 4A). We tested the ability of CDK-5 to phosphorylate the LIN-10 amino-terminus *in vitro*, using PhosTag electrophoresis to detect phosphorylated substrates based on a decrease in electrophoretic mobility (Kinoshita *et al*, 2006). Whereas CDK-5 can phosphorylate the LIN-10 amino-terminus, it could not phosphorylate a mutated version of LIN-10, LIN-10(Pmut,1–574), in which the prolines were substituted for alanines (Figure 7A).

If CDK-5 regulates LIN-10 subcellular localization by direct phosphorylation, then we would expect that mutations in the CDK-5 consensus site prolines should mimic the *cdk-5* mutant phenotype and block the effects of hypoxia and *egl-9* mutation on LIN-10 *in vivo*. We therefore introduced the identical proline to alanine substitutions into our LIN-10::GFP transgene and observed a punctate localization of the resulting LIN-10(Pmut)::GFP protein similar to that of wild-type

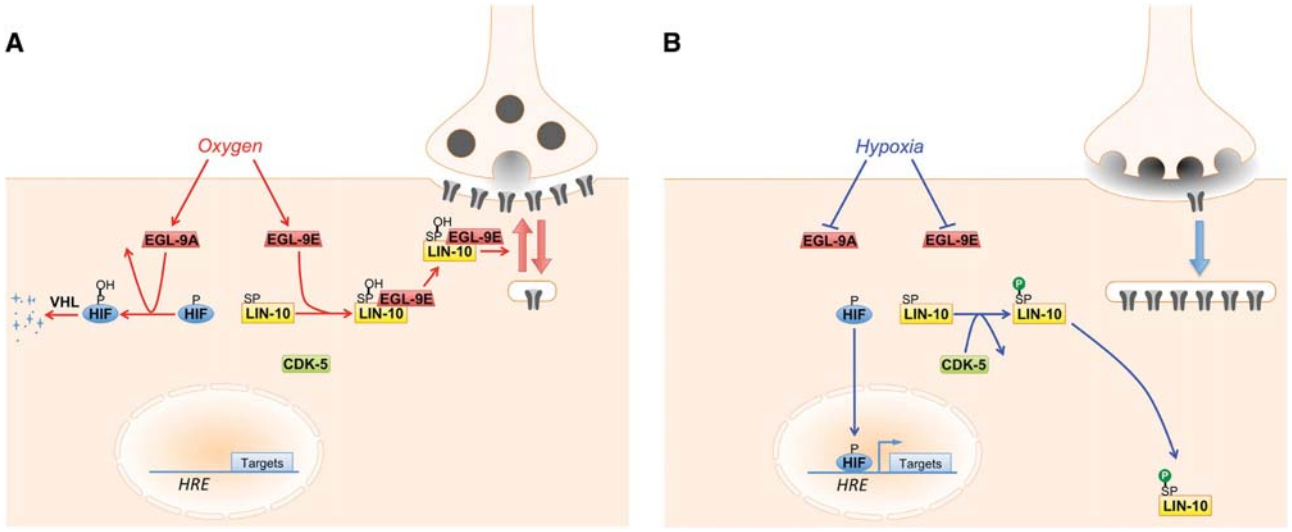

Figure 8 Model for oxygen and EGL-9 regulation of GLR-1 trafficking. (**A**) Under normal oxygen, EGL-9 (red trapezoid) regulates two targets: HIF-1 (blue ellipse) and LIN-10 (yellow rectangle). EGL-9A transiently associates with HIF-1, hydroxylating key HIF-1 prolines (indicated by 'P' and 'P-OH') on it, resulting in HIF-1 ubiquitination by VHL-1 and turnover. By contrast, EGL-9E binds to LIN-10 and drives its localization to synaptic sites and endosomes, where it promotes GLR-1 (grey channel) recycling (indicated by the two large, red arrows). We speculate that EGL-9E might also hydroxylate key prolines (CDK-5 phosphorylation sites; indicated by 'SP' and 'SP-OH') on LIN-10, or otherwise obscure CDK-5 access to these sites. (**B**) Under hypoxic conditions, both EGL-9 isoforms are inactive due to lack of oxygen. This allows HIF-1 to enter the nucleus and regulate target gene expression, although this does not impact GLR-1 localization. In addition, LIN-10 is phosphorylated by CDK-5 (green rectangle), which prevents the localization of LIN-10 at synaptic sites and endosomes. Without LIN-10 present at synaptic sites, GLR-1 recycling is depressed, tipping the balance towards internalization of GLR-1 receptors (indicated by the large blue arrow), diminished GLR-1 activity, and a change in nematode foraging behaviour. As hypoxia can trigger massive synaptic vesicle exocytosis (indicated by multiple fused synaptic vesicles at the presynaptic terminus), we also speculate that this mechanism could help protect neurons from excitotoxicity.

LIN-10::GFP (Figure 7B, D, and H). However, unlike for wild-type LIN-10::GFP, LIN-10(Pmut)::GFP remained localized in *egl-9* mutants and under conditions of hypoxia (Figure 7D, E, and H), indicating that the proline residues are required for EGL-9 and oxygen to regulate LIN-10. Importantly, neuronal expression of LIN-10(Pmut) robustly rescued the GLR-1 trafficking defects of *lin-10* mutants, indicating that the proline substitutions impaired the ability of LIN-10 to be regulated by EGL-9, CDK-5, and oxygen levels, but did not impair LIN-10 function (Figure 7I). We also examined a mutant version of LIN-10::GFP, LIN-10(S/Tmut)::GFP, in which the CDK-5 sites contain either serine or threonine to alanine substitutions (Juo *et al*, 2007). Like LIN-10(Pmut)::GFP (or wild-type LIN-10::GFP in *egl-9* mutants), LIN-10(S/Tmut)::GFP was localized even in *egl-9* mutants and hypoxic animals (Figure 7F and G). Our results indicate that phosphorylation of LIN-10 by CDK-5 disrupts LIN-10 subcellular localization, and suggest that EGL-9 regulates LIN-10 by antagonizing its phosphorylation by CDK-5 when oxygen is present, either by direct hydroxylation of key proline sites on LIN-10, or perhaps by steric hindrance of CDK-5 away from LIN-10 due to oxygen-dependent binding of EGL-9 to LIN-10. This represents a novel pathway for glutamate receptor trafficking in response to fluctuating oxygen levels.

Discussion

Here, we have shown that oxygen levels regulate GLR-1 AMPAR trafficking and GLR-1-mediated behaviour via a non-canonical variant of the hypoxia response pathway (Figure 8). When oxygen levels are sufficiently high, the EGL-9 enzyme uses dioxygen as a molecular substrate to hydroxylate a specific proline residue on HIF-1 to 4-hydroxyproline (Epstein *et al*, 2001). This modification enables VHL-1 to bind and ubiquitinate HIF-1, resulting in its proteolysis (Maxwell *et al*, 1999; Ohh *et al*, 2000; Ivan *et al*, 2001; Jaakkola *et al*, 2001; Min *et al*, 2002; Bishop *et al*, 2004; Shen *et al*, 2006). Here, we report that EGL-9 has another critical function in neurons that is independent of HIF-1: the regulation of AMPAR recycling via its interaction with LIN-10. As illustrated in Figure 8A, we favour a model in which EGL-9 uses oxygen to hydroxylate LIN-10 at prolines that comprise CDK-5 phosphorylation sites, precluding CDK-5 phosphorylation at neighbouring serine or threonine residues. In the absence of CDK-5 phosphorylation, the LIN-10 amino-terminus directs its localization to endosomes, where LIN-10 promotes GLR-1 recycling. When oxygen levels are low (Figure 8B), EGL-9 cannot hydroxylate LIN-10, thereby allowing CDK-5 to phosphorylate the LIN-10 amino-terminus and disrupt LIN-10 endosomal localization. In effect, EGL-9 and CDK-5 compete for LIN-10, with oxygen tipping the balance towards EGL-9. This mechanism keeps LIN-10 at endosomes so as to constantly resupply synapses with GLR-1 receptors when oxygen is plentiful, and it results in LIN-10 inhibition and hence GLR-1 internalization when oxygen is scarce.

The pathway by which EGL-9 regulates LIN-10 is distinct from the oxygen-dependent degradation of HIF-1 in several ways. First, the pathway is independent of HIF-1, with EGL-9 directly interacting with LIN-10 protein instead. Mutations in *hif-1* do not appear to alter GLR-1 trafficking, and mutations in *lin-10* do not appear to alter the stability of HIF-1 protein or the expression of HIF-1 target genes, indicating that these pathways function independently from one another. Second, the regulatory outcome of this pathway is at the level of a post-translational response—GLR-1 trafficking—rather than a transcriptional response. Third, in the canonical pathway,

EGL-9 is negatively regulating its target, HIF-1, whereas during the regulation of GLR-1, EGL-9 is positively regulating its target, LIN-10. Fourth, the cell biological outcome of EGL-9 activity on its target involves protein turnover in the case of HIF-1, whereas it involves altered subcellular localization in the case of LIN-10. The discovery of this novel pathway suggests that the mechanisms by which cells and prolyl hydroxylase proteins like EGL-9 respond to changes in oxygen are likely more diverse than originally appreciated.

What is the function of this novel regulation? *C. elegans*, as a soil nematode, does encounter environments of low oxygen, including the buried spaces and rotting material where it feeds on bacteria (Anderson and Dusenbery, 1977; Van Voorhies and Ward, 2000). Since *C. elegans* lack specialized respiratory structures, gaseous exchange is believed to occur through the body cuticle directly into tissues and the fluid of the pseudocoelomic body cavity. A broad range of oxygen concentration is found below the soil surface depending on variables such as aeration, temperature, moisture levels, and the bacterial population. Nematodes avoid both hyperoxic (>15% oxygen) and hypoxic (<4% oxygen) environments, showing a preference for more intermediate levels (Gray *et al*, 2004; Cheung *et al*, 2005). The neurons AQR, PQR, and URX are exposed in the body cavity and express soluble guanylate cyclases that bind and sense oxygen in the body cavity fluid; these neurons are thought to mediate a rapid aerotaxis response to changing oxygen levels (Cheung *et al*, 2004; Gray *et al*, 2004). By contrast, the EGL-9/HIF-1 canonical hypoxia response pathway is broadly expressed in *C. elegans* and is thought to elicit slower, cell-autonomous stress responses to low oxygen, but not directly mediate rapid aerotaxis responses (Branicky and Schafer, 2008). However, these two mechanisms are partly linked, as the activity of HIF-1 in *C. elegans* neurons can adjust the preferred oxygen range to which nematodes will aerotax by reorganizing the neural circuits required for oxygen sensation (Chang and Bargmann, 2008; Pocock and Hobert, 2008). Our findings here indicate that oxygen sensation and behaviour are linked by a third mechanism: the EGL-9/LIN-10/GLR-1 pathway. Under conditions of either hypoxia or loss of EGL-9 activity, there is a decrease in spontaneous reversal frequency for nematode locomotion off of food, consistent with depressed GLR-1 function. Affected animals track for longer stretches, resulting in a greater pattern of exploratory behaviour. In the case of *egl-9* mutants, reversal behaviour is fully restored when EGL-9 activity is provided back solely to the GLR-1-expressing interneurons. This would suggest that, like the AQR, PQR, and URX sensory neurons, the command interneurons also sense oxygen and modulate animal behaviour in response.

The EGL-9/LIN-10 pathway might also have a neuroprotective function. Ischaemic stroke results in nervous system damage due to local oxygen deprivation in the brain, as hypoxic neurons undergo glutamate receptor-mediated excitotoxic necrosis (Khaldi *et al*, 2002; Limbrick *et al*, 2003; Arundine and Tymianski, 2004; Mehta *et al*, 2007). It is unclear how glutamate receptors respond to such hypoxic insult. Interestingly, neurons can use homeostatic 'synaptic scaling' mechanisms to downregulate surface AMPAR expression in response to increased neural activity (Turrigiano, 2008), raising the possibility that a similar response could be triggered in ischaemic neurons. We propose that neurons likely employ multiple adaptive responses to hypoxia, and that the EGL-9/LIN-10 pathway, and perhaps a PHD/Mint orthologous pathway in mammals, might represent one such underlying neuroprotective mechanism.

Materials and methods

Transgenes and germline transformation

Transgenic strains generated in this study were isolated after microinjecting various plasmids (5–50 ng/ml) using *rol-6dm* (a gift from C Mello, UMass), *ttx-3*::*rfp* (a gift from O Hobert, Columbia Univ.), or *lin-15*(+) (a gift from J Mendel, CalTech) as a marker. Plasmids containing the *glr-1*, followed by the indicated cDNA construct, were generated using standard techniques. All resulting transgenes were introduced into the germline and followed as extrachromosomal arrays. The Phosphomutant LIN-10(S/Tmut)::GFP construct was a gift from P Juo (Tufts; termed LIN-10(10Pm)::GFP in his paper). The proline mutant LIN-10(Pmut)::GFP was created using a construct containing synthesized LIN-10 cDNA (GeneScript); the following proline residues in LIN-10 were mutated to alanine in LIN-10(Pmut): P16, 27, 29, 88, 156, 202, 331, 397, 417, and 421. These are corresponding sites for LIN-10(S/Tmut)::GFP (Juo *et al*, 2007).

Hypoxic exposure

Animals were grown at 20°C on standard NGM plates seeded with OP50 *E. coli*. For hypoxia, animals were incubated in a hypoxia chamber (C-174 chamber, Biospherix) for 24 h at 20°C and recovered in ambient oxygen for 12 h at 20°C. The oxygen level was automatically maintained with an oxygen controller (ProOx P110, Biospherix) supplied with compressed nitrogen gas.

Fluorescence microscopy

GFP- and RFP-tagged fluorescent proteins were visualized in nematodes by mounting larvae on 2% agarose pads with levamisole. Fluorescent images were observed using a Zeiss Axioplan II. A ×100 (NA = 1.4) PlanApo objective was used to detect GFP and RFP signals. Imaging was done with an ORCA charge-coupled device (CCD) camera (Hamamatsu, Bridgewater, NJ) using IPLab software (Scanalytics, Inc, Fairfax, VA) or iVision v4.0.11 (Biovision Technologies, Exton, PA) software. Exposure times were chosen to fill the 12-bit dynamic range without saturation. In most cases, maximum intensity projections of z-series stacks were obtained and out-of-focus light was removed with a constrained iterative deconvolution algorithm (iVision). For images, we captured the ventral cord dendrites in the region posterior to the RIG and AVG cell bodies.

The quantification of ventral nerve cord fluorescent objects (i.e., puncta and elongated compartments) was done using ImageJ (Collins, 2007) to automatically threshold the images and then determine the outlines of fluorescent objects in ventral cord dendrites. ImageJ was used to quantify both the shape and the size of all individual fluorescent objects along the ventral cord. This allowed us to distinguish between the small GLR-1::GFP puncta in wild-type animals and the large, aberrant compartments (which have an elongated shape rarely observed in wild type) in hypoxic animals, as well as in *egl-9* and *lin-10* mutants. Object size was measured as the maximum diameter for each outlined puncta. Object number was calculated by counting the average number of puncta per 100 microns of dendrite length. The amount of a given fluorescent protein per puncta was calculated by summing all of the pixel values contained within each individual punctum to yield an IOD score for each punctum.

Behavioural assays

The reversal frequency of individual animals was assayed as previously described, but with some modifications (Zheng *et al*, 1999). Single young adult hermaphrodites were placed on NGM plates in the absence of food. The animals were allowed to adjust to the plates for 5 min, and the number of spontaneous reversals for each animal was counted over a 5-min period. Twenty or more animals were tested for each genotype, and the reported scores reflect the mean number of reversals per minute, normalized as a percentage of the value of wild-type controls. Nose-touch mechanosensation was assayed by placing young adult hermaphrodites on

NGM plates with food. Individual young adult animals were allowed to collide with a human hair 10 consecutive times within a 5-min period. Activation of the reversal behaviour was scored immediately after each contact with the hair stimulus and the score summed over the 10 trials. Twenty or more animals were tested for each genotype, and the reported scores reflect the mean number of responses.

Patch-clamp whole-cell recording

In-vivo whole-cell recordings were carried out at room temperature with an EPC-10 amplifier and Patchmaster software (HEKA) using a protocol described in a previous study (Wang *et al*, 2008; Ward *et al*, 2008). Briefly, the head of glued worms was dissected and the AVA neurons were exposed for patch-clamp recordings in the bath solution. Recording pipettes were pulled from borosilicate glass. The pipette solution contained 115 mM K-gluconate, 25 mM KCl, 50 mM HEPES, 0.1 mM $CaCl_2$, 1 mM BAPTA, 5 mM MgATP, 0.5 mM NaGTP (315 mOsm, pH adjusted to 7.35 with KOH). The bath solution contained 150 mM NaCl, 5 mM KCl, 5 mM $CaCl_2$, 1 mM $MgCl_2$, 15 mM HEPES, 10 mM Glucose (325 mOsm, pH adjusted to 7.35 with KOH). Voltages were clamped at −70 mV. Current data were sampled at 22 kHz. In all, 1 mM glutamate was applied for 1 s by pressure ejection.

Immunolabelling of cell surface

Cell surfaces along the ventral nerve cord in transgenic animals expressing HA::GLR-1::GFP (a gift from AV Maricq, Univ. of Utah) were immunolabelled as described (Gottschalk and Schafer, 2006). Briefly, AlexaFluor594-conjugated mouse monoclonal anti-HA antibodies (Molecular Probes) were 200-fold diluted in injection buffer (20 mM K_3PO_4, 3 mM K citrate, 2% PEG 6000, pH 7.5) and injected into the pseudocoelomic space of transgenic animals. After a 5 h of recovery, animals were mounted and observed for epifluorescence as described above.

Immunodetection of LIN-10

To measure LIN-10::GFP protein levels, 30 young adults of each wild type and mutants expressing the *odIs22* transgene were dissolved in 1 × Laemmli buffer by fresh freezing and boiling for 10 min. To observe phosphorylation, the amino-terminal half of wild-type and proline-mutant LIN-10 (amino acids 1–574) was N-terminally tagged with FLAG, expressed in rabbit reticulocyte-based protein expression system (Promega). *In vitro*-expressed proteins were incubated in kinase buffer (50 mM HEPES, pH 7, 10 mM $MgCl_2$, 100 μm ATP, 1 mM dithiothreitol, 50 mM β-glycerolphosphate) for 30 min at 37°C either with or without recombinant CDK5/p25 (Millipore). Reactions were stopped by adding Laemmli buffer and analysed onto 10% SDS–polyacrylamide gels containing 30 mM Phos-tag AAL-107 (Nard Institute, Japan). Western blotting was performed using mouse anti-GFP (1:1000, Roche), mouse anti-Actin (1:2000, MP Biomedicals), and mouse anti-Flag (1:3000, Sigma).

Yeast two-hybrid interactions

A yeast two-hybrid bait plasmid containing just the catalytic domain of EGL-9 (amino acids 347–608) was generated so as to screen a *C. elegans* cDNA library in pGAD-GH (David Sherwood, Duke University). Transformed yeast were selected for interaction on –Trp –Leu plates; 3 470 000 transformed colonies were screened, resulting in 40 His+ positives. Candidates were tested for β galactosidase activity, yielding 19 positive clones with in-frame cDNA inserts.

To confirm the interactions between LIN-10 and EGL-9, corresponding cDNAs were introduced into the Matchmaker™ GAL4 Two-Hybrid System 3 (Clontech, Palo Alto, CA), which uses four reporter genes: *HIS3*, *ADE2*, *MEL1* (α galactosidase), and *lacZ* (β galactosidase). Transformed yeast was selected on –His –Trp –Leu plates. Twenty colonies were selected for serial dilution analysis on –His –Trp –Leu –Ade plates containing X-α galactoside, or were assayed for β galactosidase activity on filters. Strong growth was indicated by activation of all four reporters. Weak growth was indicated by activation of at least three reporters.

Supplementary data

Supplementary data are available at *The EMBO Journal* Online (http://www.embojournal.org).

Acknowledgements

We thank Andy Fire, the *C. elegans* Genetics Center, Villu Maricq, Joshua Kaplan, Peter Juo, Shohei Mitani, and Richard Tsien for reagents and strains. We thank Maureen Barr, Barth Grant, Monica Driscoll, Natalia Morsci, Doreen Glodowski, and Indrani Chatterjee for comments on the manuscript. This work was supported by National Institutes of Health (NIH) R01 NS42023 and a State of New Jersey Brain Injury Research Grant (07-3201-BIR-E-1) to CR, NIH R01 GM78424 to JAP-C, a State of New Jersey Spinal Cord Postdoctoral Research Fellowship (10-2950-SCR-E-0) to ECP, and an NIH F31 NS071741 Fellowship and Waksman Benedict Michael Fellowship to PG.

Author contributions: ECP and PG designed and performed the genetic, molecular, behavioural, and cell biological experiments under the direct supervision of CR, with each author making equal contributions. LK and SX performed the electrophysiological recordings. ZS, QY, and JAP-C designed and performed the yeast two-hybrid analysis of LIN-10/EGL-9 interactions. PG, ECP, and CR wrote the manuscript, with significant editorial input and discussion of the results and their implications at all stages of the process from JAP-C.

Conflict of interest

The authors declare that they have no conflict of interest.

References

Anderson GL, Dusenbery DB (1977) Critical-oxygen tension of Caenorhabditis elegans. *J Nematol* **9:** 253–254

Aragones J, Fraisl P, Baes M, Carmeliet P (2009) Oxygen sensors at the crossroad of metabolism. *Cell Metab* **9:** 11–22

Arundine M, Tymianski M (2004) Molecular mechanisms of glutamate-dependent neurodegeneration in ischemia and traumatic brain injury. *Cell Mol Life Sci* **61:** 657–668

Bishop T, Lau KW, Epstein AC, Kim SK, Jiang M, O'Rourke D, Pugh CW, Gleadle JM, Taylor MS, Hodgkin J, Ratcliffe PJ (2004) Genetic analysis of pathways regulated by the von Hippel-Lindau tumor suppressor in Caenorhabditis elegans. *PLoS Biol* **2:** e289

Branicky RS, Schafer WR (2008) Oxygen homeostasis: how the worm adapts to variable oxygen levels. *Curr Biol* **18:** R559–R560

Bruick RK, McKnight SL (2001) A conserved family of prolyl-4-hydroxylases that modify HIF. *Science (New York, NY)* **294:** 1337–1340

Buchan AM, Li H, Cho S, Pulsinelli WA (1991) Blockade of the AMPA receptor prevents CA1 hippocampal injury following severe but transient forebrain ischemia in adult rats. *Neurosci Lett* **132:** 255–258

Burbea M, Dreier L, Dittman JS, Grunwald ME, Kaplan JM (2002) Ubiquitin and AP180 regulate the abundance of GLR-1 glutamate receptors at postsynaptic elements in C. elegans. *Neuron* **35:** 107–120

Chang AJ, Bargmann CI (2008) Hypoxia and the HIF-1 transcriptional pathway reorganize a neuronal circuit for oxygen-dependent behavior in Caenorhabditis elegans. *Proc Natl Acad Sci USA* **105:** 7321–7326

Chang HC, Rongo C (2005) Cytosolic tail sequences and subunit interactions are critical for synaptic localization of glutamate receptors. *J Cell Sci* **118**(Part 9)**:** 1945–1956

Cheung BH, Arellano-Carbajal F, Rybicki I, de Bono M (2004) Soluble guanylate cyclases act in neurons exposed to the body fluid to promote C. elegans aggregation behavior. *Curr Biol* **14:** 1105–1111

Cheung BH, Cohen M, Rogers C, Albayram O, de Bono M (2005) Experience-dependent modulation of C. elegans behavior by ambient oxygen. *Curr Biol* **15:** 905–917

Chowdhury R, McDonough MA, Mecinovic J, Loenarz C, Flashman E, Hewitson KS, Domene C, Schofield CJ (2009) Structural basis

for binding of hypoxia-inducible factor to the oxygen-sensing prolyl hydroxylases. *Structure* **17:** 981–989

Collins TJ (2007) ImageJ for microscopy. *BioTechniques* **43** (1 Suppl)**:** 25–30

Cummins EP, Berra E, Comerford KM, Ginouves A, Fitzgerald KT, Seeballuck F, Godson C, Nielsen JE, Moynagh P, Pouyssegur J, Taylor CT (2006) Prolyl hydroxylase-1 negatively regulates IkappaB kinase-beta, giving insight into hypoxia-induced NFkappaB activity. *Proc Natl Acad Sci USA* **103:** 18154–18159

Darby C, Cosma CL, Thomas JH, Manoil C (1999) Lethal paralysis of Caenorhabditis elegans by Pseudomonas aeruginosa. *Proc Natl Acad Sci USA* **96:** 15202–15207

Emtage L, Chang H, Tiver R, Rongo C (2009) MAGI-1 modulates AMPA receptor synaptic localization and behavioral plasticity in response to prior experience. *PloS One* **4:** e4613

Epstein AC, Gleadle JM, McNeill LA, Hewitson KS, O'Rourke J, Mole DR, Mukherji M, Metzen E, Wilson MI, Dhanda A, Tian YM, Masson N, Hamilton DL, Jaakkola P, Barstead R, Hodgkin J, Maxwell PH, Pugh CW, Schofield CJ, Ratcliffe PJ (2001) C. elegans EGL-9 and mammalian homologs define a family of dioxygenases that regulate HIF by prolyl hydroxylation. *Cell* **107:** 43–54

Fandrey J, Gassmann M (2009) Oxygen sensing and the activation of the hypoxia inducible factor 1 (HIF-1)—invited article. *Adv Exp Med Biol* **648:** 197–206

Fong GH, Takeda K (2008) Role and regulation of prolyl hydroxylase domain proteins. *Cell Death Differ* **15:** 635–641

Fu J, Menzies K, Freeman RS, Taubman MB (2007) EGLN3 prolyl hydroxylase regulates skeletal muscle differentiation and myogenin protein stability. *J Biol Chem* **282:** 12410–12418

Fu J, Taubman MB (2010) Prolyl hydroxylase EGLN3 regulates skeletal myoblast differentiation through an NF-kappaB-dependent pathway. *J Biol Chem* **285:** 8927–8935

Gill R (1994) The pharmacology of alpha-amino-3-hydroxy-5-methyl-4-isoxazole propionate (AMPA)/kainate antagonists and their role in cerebral ischaemia. *Cerebrovasc Brain Metab Rev* **6:** 225–256

Glodowski DR, Chen CC, Schaefer H, Grant BD, Rongo C (2007) RAB-10 regulates glutamate receptor recycling in a cholesterol-dependent endocytosis pathway. *Mol Biol Cell* **18:** 4387–4396

Glodowski DR, Wright T, Martinowich K, Chang HC, Beach D, Rongo C (2005) Distinct LIN-10 domains are required for its neuronal function, its epithelial function, and its synaptic localization. *Mol Biol Cell* **16:** 1417–1426

Gort EH, van Haaften G, Verlaan I, Groot AJ, Plasterk RH, Shvarts A, Suijkerbuijk KP, van Laar T, van der Wall E, Raman V, van Diest PJ, Tijsterman M, Vooijs M (2008) The TWIST1 oncogene is a direct target of hypoxia-inducible factor-2alpha. *Oncogene* **27:** 1501–1510

Gottschalk A, Schafer WR (2006) Visualization of integral and peripheral cell surface proteins in live Caenorhabditis elegans. *J Neurosci Methods* **154:** 68–79

Gray JM, Karow DS, Lu H, Chang AJ, Chang JS, Ellis RE, Marletta MA, Bargmann CI (2004) Oxygen sensation and social feeding mediated by a C. elegans guanylate cyclase homologue. *Nature* **430:** 317–322

Grunwald ME, Mellem JE, Strutz N, Maricq AV, Kaplan JM (2004) Clathrin-mediated endocytosis is required for compensatory regulation of GLR-1 glutamate receptors after activity blockade. *Proc Natl Acad Sci USA* **101:** 3190–3195

Hart AC, Sims S, Kaplan JM (1995) Synaptic code for sensory modalities revealed by *C. elegans* GLR-1 glutamate receptor. *Nature* **378:** 82–84

Hayashi Y, Shi SH, Esteban JA, Piccini A, Poncer JC, Malinow R (2000) Driving AMPA receptors into synapses by LTP and CaMKII: requirement for GluR1 and PDZ domain interaction. *Science (New York, NY)* **287:** 2262–2267

Ivan M, Kondo K, Yang H, Kim W, Valiando J, Ohh M, Salic A, Asara JM, Lane WS, Kaelin Jr WG (2001) HIFalpha targeted for VHL-mediated destruction by proline hydroxylation: implications for O2 sensing. *Science (New York, NY)* **292:** 464–468

Jaakkola P, Mole DR, Tian YM, Wilson MI, Gielbert J, Gaskell SJ, Kriegsheim A, Hebestreit HF, Mukherji M, Schofield CJ, Maxwell PH, Pugh CW, Ratcliffe PJ (2001) Targeting of HIF-alpha to the von Hippel-Lindau ubiquitylation complex by O2-regulated prolyl hydroxylation. *Science (New York, NY)* **292:** 468–472

Jiang H, Guo R, Powell-Coffman JA (2001) The Caenorhabditis elegans hif-1 gene encodes a bHLH-PAS protein that is required for adaptation to hypoxia. *Proc Natl Acad Sci USA* **98:** 7916–7921

Juo P, Harbaugh T, Garriga G, Kaplan JM (2007) CDK-5 regulates the abundance of GLR-1 glutamate receptors in the ventral cord of Caenorhabditis elegans. *Mol Biol Cell* **18:** 3883–3893

Khaldi A, Chiueh CC, Bullock MR, Woodward JJ (2002) The significance of nitric oxide production in the brain after injury. *Ann NY Acad Sci* **962:** 53–59

Kinoshita E, Kinoshita-Kikuta E, Takiyama K, Koike T (2006) Phosphate-binding tag, a new tool to visualize phosphorylated proteins. *Mol Cell Proteomics* **5:** 749–757

Koditz J, Nesper J, Wottawa M, Stiehl DP, Camenisch G, Franke C, Myllyharju J, Wenger RH, Katschinski DM (2007) Oxygen-dependent ATF-4 stability is mediated by the PHD3 oxygen sensor. *Blood* **110:** 3610–3617

Kramer LB, Shim J, Previtera ML, Isack NR, Lee MC, Firestein BL, Rongo C (2010) UEV-1 is an ubiquitin-conjugating enzyme variant that regulates glutamate receptor trafficking in C. elegans neurons. *PloS One* **5:** e14291

Lee S, Nakamura E, Yang H, Wei W, Linggi MS, Sajan MP, Farese RV, Freeman RS, Carter BD, Kaelin Jr WG, Schlisio S (2005) Neuronal apoptosis linked to EglN3 prolyl hydroxylase and familial pheochromocytoma genes: developmental culling and cancer. *Cancer Cell* **8:** 155–167

Lees GJ (2000) Pharmacology of AMPA/kainate receptor ligands and their therapeutic potential in neurological and psychiatric disorders. *Drugs* **59:** 33–78

Li H, Buchan AM (1993) Treatment with an AMPA antagonist 12 hours following severe normothermic forebrain ischemia prevents CA1 neuronal injury. *J Cereb Blood Flow Metab* **13:** 933–939

Limbrick Jr DD, Sombati S, DeLorenzo RJ (2003) Calcium influx constitutes the ionic basis for the maintenance of glutamate-induced extended neuronal depolarization associated with hippocampal neuronal death. *Cell Calcium* **33:** 69–81

Lissin DV, Carroll RC, Nicoll RA, Malenka RC, von Zastrow M (1999) Rapid, activation-induced redistribution of ionotropic glutamate receptors in cultured hippocampal neurons [published erratum appears in J Neurosci 1999 Apr 15;19(8):3275]. *J Neurosci* **19:** 1263–1272

Lissin DV, Gomperts SN, Carroll RC, Christine CW, Kalman D, Kitamura M, Hardy S, Nicoll RA, Malenka RC, von Zastrow M (1998) Activity differentially regulates the surface expression of synaptic AMPA and NMDA glutamate receptors. *Proc Natl Acad Sci USA* **95:** 7097–7102

Mammen AL, Kameyama K, Roche KW, Huganir RL (1997) Phosphorylation of the alpha-amino-3-hydroxy-5-methylisoxazole4-propionic acid receptor GluR1 subunit by calcium/calmodulin-dependent kinase II. *J Biol Chem* **272:** 32528–32533

Maricq AV, Peckol E, Driscoll M, Bargmann CI (1995) Mechanosensory signalling in *C. elegans* mediated by the GLR-1 glutamate receptor. *Nature* **378:** 78–81

Maxwell PH, Wiesener MS, Chang GW, Clifford SC, Vaux EC, Cockman ME, Wykoff CC, Pugh CW, Maher ER, Ratcliffe PJ (1999) The tumour suppressor protein VHL targets hypoxia-inducible factors for oxygen-dependent proteolysis. *Nature* **399:** 271–275

McDonough MA, Li V, Flashman E, Chowdhury R, Mohr C, Lienard BM, Zondlo J, Oldham NJ, Clifton IJ, Lewis J, McNeill LA, Kurzeja RJ, Hewitson KS, Yang E, Jordan S, Syed RS, Schofield CJ (2006) Cellular oxygen sensing: crystal structure of hypoxia-inducible factor prolyl hydroxylase (PHD2). *Proc Natl Acad Sci USA* **103:** 9814–9819

Mehta SL, Manhas N, Raghubir R (2007) Molecular targets in cerebral ischemia for developing novel therapeutics. *Brain Res Rev* **54:** 34–66

Mellem JE, Brockie PJ, Zheng Y, Madsen DM, Maricq AV (2002) Decoding of polymodal sensory stimuli by postsynaptic glutamate receptors in *C. elegans*. *Neuron* **36:** 933–944

Min JH, Yang H, Ivan M, Gertler F, Kaelin Jr WG, Pavletich NP (2002) Structure of an HIF-1alpha-pVHL complex: hydroxyproline recognition in signaling. *Science (New York, NY)* **296:** 1886–1889

Nellgard B, Wieloch T (1992) Postischemic blockade of AMPA but not NMDA receptors mitigates neuronal damage in the rat brain following transient severe cerebral ischemia. *J Cereb Blood Flow Metab* **12:** 2–11

'O'Brien RJ, Kamboj S, Ehlers MD, Rosen KR, Fischbach GD, Huganir RL (1998) Activity-dependent modulation of synaptic AMPA receptor accumulation [see comments]. *Neuron* **21:** 1067–1078

Ohh M, Park CW, Ivan M, Hoffman MA, Kim TY, Huang LE, Pavletich N, Chau V, Kaelin WG (2000) Ubiquitination of hypoxia-inducible factor requires direct binding to the beta-domain of the von Hippel-Lindau protein. *Nat Cell Biol* **2:** 423–427

Pamenter ME, Shin DS, Cooray M, Buck LT (2008) Mitochondrial ATP-sensitive K+ channels regulate NMDAR activity in the cortex of the anoxic western painted turtle. *J Physiol* **586:** 1043–1058

Park EC, Glodowski DR, Rongo C (2009) The ubiquitin ligase RPM-1 and the p38 MAPK PMK-3 regulate AMPA receptor trafficking. *PloS One* **4:** e4284

Pocock R, Hobert O (2008) Oxygen levels affect axon guidance and neuronal migration in Caenorhabditis elegans. *Nat Neurosci* **11:** 894–900

Rizo J, Sudhof TC (1998) C2-domains, structure and function of a universal Ca2+-binding domain. *J Biol Chem* **273:** 15879–15882

Rongo C, Kaplan JK (1999) CaMKII regulates the density of central glutamatergic synapses *in vivo*. *Nature* **402:** 195–199

Rongo C, Whitfield CW, Rodal A, Kim SK, Kaplan JM (1998) LIN-10 is a shared component of the polarized protein localization pathways in neurons and epithelia. *Cell* **94:** 751–759

Schaefer H, Rongo C (2006) KEL-8 is a substrate receptor for CUL3-dependent ubiquitin ligase that regulates synaptic glutamate receptor turnover. *Mol Biol Cell* **17:** 1250–1260

Semenza GL (2009) Regulation of oxygen homeostasis by hypoxia-inducible factor 1. *Physiology (Bethesda)* **24:** 97–106

Shao Z, Zhang Y, Powell-Coffman JA (2009) Two distinct roles for EGL-9 in the regulation of HIF-1-mediated gene expression in Caenorhabditis elegans. *Genetics* **183:** 821–829

Shao Z, Zhang Y, Ye Q, Saldanha JN, Powell-Coffman JA (2010) C. elegans SWAN-1 binds to EGL-9 and regulates HIF-1-mediated resistance to the bacterial pathogen Pseudomonas aeruginosa PAO1. *PLoS Pathog* **6:** e1001075

Sheardown MJ, Suzdak PD, Nordholm L (1993) AMPA, but not NMDA, receptor antagonism is neuroprotective in gerbil global ischaemia, even when delayed 24 h. *Eur J Pharmacol* **236:** 347–353

Shen C, Shao Z, Powell-Coffman JA (2006) The Caenorhabditis elegans rhy-1 gene inhibits HIF-1 hypoxia-inducible factor activity in a negative feedback loop that does not include vhl-1. *Genetics* **174:** 1205–1214

Shi A, Chen CC, Banerjee R, Glodowski D, Audhya A, Rongo C, Grant BD (2010) EHBP-1 functions with RAB-10 during endocytic recycling in Caenorhabditis elegans. *Mol Biol Cell* **21:** 2930–2943

Shi SH, Hayashi Y, Petralia RS, Zaman SH, Wenthold RJ, Svoboda K, Malinow R (1999) Rapid spine delivery and redistribution of AMPA receptors after synaptic NMDA receptor activation. *Science (New York, NY)* **284:** 1811–1816

Shim J, Umemura T, Nothstein E, Rongo C (2004) The unfolded protein response regulates glutamate receptor export from the endoplasmic reticulum. *Mol Biol Cell* **15:** 4818–4828

Shin DS, Buck LT (2003) Effect of anoxia and pharmacological anoxia on whole-cell NMDA receptor currents in cortical neurons from the western painted turtle. *Physiol Biochem Zool* **76:** 41–51

Takahashi M, Kohara A, Shishikura J, Kawasaki-Yatsugi S, Ni JW, Yatsugi S, Sakamoto S, Okada M, Shimizu-Sasamata M, Yamaguchi T (2002) YM872: a selective, potent and highly water-soluble alpha-amino-3-hydroxy-5-methylisoxazole-4-propionic acid receptor antagonist. *CNS Drug Rev* **8:** 337–352

Turrigiano GG (2008) The self-tuning neuron: synaptic scaling of excitatory synapses. *Cell* **135:** 422–435

Van Voorhies WA, Ward S (2000) Broad oxygen tolerance in the nematode Caenorhabditis elegans. *J Exp Biol* **203**(Part 16)**:** 2467–2478

Wang GJ, Kang L, Kim JE, Maro GS, Xu XZ, Shen K (2010) GRLD-1 regulates cell-wide abundance of glutamate receptor through post-transcriptional regulation. *Nat Neurosci* **13:** 1489–1495

Wang R, Walker CS, Brockie PJ, Francis MM, Mellem JE, Madsen DM, Maricq AV (2008) Evolutionary conserved role for TARPs in the gating of glutamate receptors and tuning of synaptic function. *Neuron* **59:** 997–1008

Ward A, Liu J, Feng Z, Xu XZ (2008) Light-sensitive neurons and channels mediate phototaxis in C. elegans. *Nat Neurosci* **11:** 916–922

Whitfield CW, Benard C, Barnes T, Hekimi S, Kim SK (1999) Basolateral localization of the *Caenorhabditis elegans* epidermal growth factor receptor in epithelial cells by the PDZ protein LIN-10. *Mol Biol Cell* **10:** 2087–2100

Xue D, Huang ZG, Barnes K, Lesiuk HJ, Smith KE, Buchan AM (1994) Delayed treatment with AMPA, but not NMDA, antagonists reduces neocortical infarction. *J Cereb Blood Flow Metab* **14:** 251–261

Zheng Y, Brockie PJ, Mellem JE, Madsen DM, Maricq AV (1999) Neuronal control of locomotion in C. elegans is modified by a dominant mutation in the GLR-1 ionotropic glutamate receptor. *Neuron* **24:** 347–361

Zivkovic G, Buck LT (2010) Regulation of AMPA receptor currents by mitochondrial ATP-sensitive K+ channels in anoxic turtle neurons. *J Neurophysiol* **104:** 1913–1922